Received: 17 June 2021 | Revised: 10 September 2021 | Accepted: 19 September 2021

DOI: 10.1002/bit.27996

ARTICLE

BIOTECHNOLOGY AND BIOENGINEERING WILEY

IR780 loaded gelatin-PEG coated gold core silica shell nanorods for cancer-targeted photothermal/photodynamic therapy

Ariana S. C. Gonçalves[1] | Carolina F. Rodrigues[1] | Natanael Fernandes[1] | Duarte de Melo-Diogo[1] | Paula Ferreira[2] | André F. Moreira[1] | Ilídio J. Correia[1,2]

[1]CICS-UBI – Health Sciences Research Centre, Universidade da Beira Interior, Covilhã, Portugal

[2]CIEPQPF – Departamento de Engenharia Química, Universidade de Coimbra, Coimbra, Portugal

Correspondence

André F. Moreira and Ilídio J. Correia, CICS-UBI – Health Sciences Research Centre, Universidade da Beira Interior, Av Infante D Henrique, 6200-506 Covilhã, Portugal.
Email: afmoreira@fcsaude.ubi.pt and icorreia@ubi.pt

Funding information

European Regional Development Fund, Grant/Award Numbers: CENTRO-01-0145-FEDER-028989, POCI-01-0145-FEDER-031462; Fundação para a Ciência e a Tecnologia, Grant/Award Numbers: SFRH/BD/144680/2019, UIDB/00709/2020

Abstract

Gold core silica shell (AuMSS) nanorods present excellent physicochemical properties that allow their application as photothermal and drug delivery agents. Herein, AuMSS nanorods were dual-functionalized with Polyethylene glycol methyl ether (PEG-CH_3) and Gelatin (GEL) to enhance both the colloidal stability and uptake by HeLa cancer cells. Additionally, the AuMSS nanorods were combined for the first time with IR780 (a heptamethine cyanine molecule) and its photothermal and photodynamic capacities were determined. The obtained results reveal that the encapsulation of IR780 (65 µg per AuMSS mg) increases the photothermal conversion efficiency of AuMSS nanorods by 10%, and this enhanced heat generation was maintained even after three irradiation cycles with a NIR (808 nm) laser. Moreover, the IR780-loaded AuMSS/T-PEG-CH_3/T-GEL presented ≈2-times higher uptake in HeLa cells, when compared to the non-coated counterparts, and successfully mediated the light-triggered generation of reactive oxygen species. Overall, the combination of photodynamic and photothermal therapy mediated by IR780-loaded AuMSS/T-PEG-CH_3/T-GEL nanorods effectively promoted the ablation of HeLa cancer cells.

KEYWORDS

Gelatin, gold core silica shell nanoparticles, IR780, PEG-CH_3, photodynamic therapy, photothermal therapy

1 | INTRODUCTION

Photothermal therapy (PTT) has been widely studied as a new anticancer approach (Fernandes et al., 2020; Huang et al., 2008). This therapy explores the increment of the tumor tissue' temperature, to values above 42°C, to sensitize the cancer cells to the action of other therapeutics (e.g., chemotherapy) or even to induce its death (de Melo-Diogo et al., 2017). The PTT mediated by nanoparticles takes advantage of the nanoparticles' reduced size and ability to accumulate in the tumor tissue. Once in the tumor, the nanoparticles are activated by the irradiation with near-infrared (NIR) light (700–1000 nm), converting the energy of irradiated light into heat (Fernandes et al., 2020; Moreira et al., 2016). Therefore, the nanoparticles allow superior control over the hyperthermia, producing an on-demand temperature increase confined to the tumor tissue and reducing the side effects (Gonçalves et al., 2020). Several types of nanoparticles can be applied as photothermal agents, such as those composed of gold and graphene oxide, or even containing small

molecules (e.g., IR780, indocyanine green [ICG]; Alves et al., 2019; de Melo-Diogo et al., 2019; Jiang et al., 2020; Rodrigues, Reis, et al., 2019). Among them, gold nanoparticles possess unique physicochemical properties that make them one of the most explored nanoplatforms in PTT (Gonçalves et al., 2020; X. Yang et al., 2015). Gold nanoparticles present high variability in terms of shape, size, and high resistance to degradation and oxidation (Moreira, Rodrigues, Reis, Costa, & Correia, 2018). Moreover, their unique optical properties prompt their application as photothermal and bioimaging agents. Additionally, strong absorption in the NIR region can be obtained by fine-tuning the localized surface plasmon resonance phenomenon through the optimization of the gold nanoparticles' size and shape (Gonçalves et al., 2020; Moreira, Rodrigues, Reis, Costa, & Correia, 2018). Furthermore, the incorporation of a mesoporous silica shell improves the gold nanoparticles' colloidal stability and biocompatibility as well as allows diverse surface modifications (Reis et al., 2019). The mesoporous structure also facilitates the loading of therapeutic molecules protecting them from premature degradation and clearance from the human body (Rodrigues, Jacinto, et al., 2019) Additionally, the silica protects the gold-core from particle's reshaping phenomena upon exposition to high-intensity radiations (e.g., NIR laser during PTT) and its optical transparency to NIR radiation does not compromise the triggering of PTT (Gonçalves et al., 2020).

Otherwise, the effectiveness of gold-core silica shell (AuMSS) nanorods can be further improved by loading therapeutic molecules in the silica mesopores (Liu et al., 2015). The IR780 is a small molecule with an absorption peak at 780 nm that can mediate the generation of reactive oxygen species (ROS - photodynamic therapy [PDT]) and heat (PTT) upon irradiation with NIR light (Leitão et al., 2020). However, this small molecule presents poor solubility, low tumor uptake, rapid blood clearance, and acute toxicity (Alves et al., 2018). Therefore, the encapsulation of IR780 in different nanostructures has been explored to improve its solubility and tumor accumulation (Alves et al., 2018; Leitão et al., 2020).

In this study, the encapsulation of IR780 in AuMSS nanorods was explored, to the best of our knowledge for the first time, to improve the AuMSS photothermal capacity and overall therapeutic potential (i.e., combination of photodynamic and photothermal therapies). Simultaneously, a novel surface functionalization composed of Poly (ethylene glycol) methyl ether (PEG-CH_3) and Gelatin (GEL) was explored to improve the blood circulation time and the tumor-targeting capacity of AuMSS nanorods. PEG-CH_3 is a biocompatible and amphiphilic polymer that can act as a solubilizer agent to improve the colloidal stability and blood circulation time (Harris & Chess, 2003; Hussain et al., 2019). Such is attributed to the PEG capacity to decrease the adsorption of proteins on the surface of nanoparticles, reducing their recognition by the immune system and consequent elimination (Pelaz et al., 2015). Further, increased blood circulation times have been correlated with higher probabilities of the nanoparticles accumulating in the tumor tissue (Fox et al., 2009). Additionally, GEL is a natural polymer obtained through the hydrolysis of collagen with biodegradability and biocompatibility properties (Gómez-Guillén et al., 2011; Hoque et al., 2015). Moreover, GEL has specific binding domains, known as RGD sequences, with specificity to $\alpha v\beta_3$ integrin receptors, which are commonly found overexpressed in cancer cells (Davidenko et al., 2016; Su et al., 2020). Therefore, the incorporation of GEL will improve the specificity of AuMSS nanoparticles towards the cancer cells and consequently its therapeutic potential (Danhier et al., 2012; Hoch et al., 2012). The functionalization of rod-shaped AuMSS nanoparticles was achieved through a post-synthesis methodology, promoting the condensation of PEG-CH_3 and GEL silanated derivatives in the particle surface. The polymers coating neutralized the nanoparticles' surface charge and improved the AuMSS nanorods specificity and uptake by cancer cells. Additionally, the therapeutic potential of the AuMSS/IR780 combination was characterized, particularly the capacity to perform both PTT and PDT in cancer cells.

2 | MATERIALS AND METHODS

2.1 | Materials

Hydrogen tetrachloroaurate (III) hydrate ($HAuCl_4$) was purchased from Alfa Aesar. Tetraethylorthosilicate (TEOS) and tetrahydrofuran (THF) were obtained from Acros Organics. Cetyltrimethylammonium bromide (CTAB) was acquired from Tokyo Chemical Industry. Hydrochloric acid (HCl) was acquired from Panreac. Methanol was obtained from VWR International. L-ascorbic acid, silver nitrate ($AgNO_3$), Dulbecco's modified Eagle's medium-high glucose (DMEM-HG), Dulbecco's modified Eagle's medium/nutrient mixture F-12 (DMEM-F12), ethanol (EtOH), fluorescein 5-isothiocyanate (FITC), resazurin, sodium borohydride ($NaBH_4$), paraformaldehyde (PFA), PBS solution, PEG-CH_3 ($Mw = 223.35\ g\ mol^{-1}$), 3-(triethoxysilyl) propyl isocyanate (TESPIC), GEL, IR780 iodide, 2′,7′-dichlorofluorescein diacetate (H_2DCF-DA), and trypsin were bought from Sigma-Aldrich. Hoechst 33342®, calcein acetozxmethyl (Calcein AM), propidium iodide (PI), and wheat germ agglutinin conjugate Alexa 594® (WGA-Alexa Fluor® 594) were obtained from Invitrogen. Human negroid cervix epithelioid carcinoma HeLa cells (ATCCs CCL-2™) were acquired from ATCC. Primary normal human dermal fibroblast (FibH) cells were bought to Promocell. Fetal bovine serum (FBS) was acquired from Biochrom AG. Cell imaging plates were acquired from Ibidi GmbH (Ibidi). Cell culture t-flasks were supplied by Orange Scientific (Braine-l'Alleud). Double deionized and filtered water (ultrapure water) was obtained by using a Milli-Q Advantage A10 Ultrapure Water Purification System (0.22 µm filtered; 18.2 MΩ cm^{-1} at 25°C).

2.2 | Methods

2.2.1 | Synthesis of AuMSS nanorods

The rod-shaped gold nanoparticles were synthesized through a seed-mediated growth methodology, as previously described in the

literature (Jacinto et al., 2020; Rodrigues, Reis, et al., 2019). In the first step, a solution containing small spherical gold spheres (seeds) was prepared by adding 0.6 ml of $NaBH_4$ (0.01 M) to an aqueous solution containing 5 ml of CTAB (0.20 M) and 5 ml of $HAuCl_4$ (0.0005 M). After 6 h at 30°C, the seed solution was added to a growth solution, which was prepared by adding under magnetic stirring 0.21 ml of L-ascorbic acid (0.08 M), 0.03 ml of $AgNO_3$ (0.1 M), and 0.3 ml $HAuCl_4$ (0.05 M) to an aqueous solution containing 20 ml of CTAB (0.2 M). The final solution was left under magnetic stirring at 30°C for 16 h, to obtain the gold nanorods.

Then, the synthesis of the mesoporous silica shell was performed according to a method previously described in the literature (Dias et al., 2016). For that purpose, the gold nanorods were centrifuged (12,000*g*, 20 min at 25°C) to remove the excess of CTAB and resuspended in ultrapure water. Subsequently, 0.7 ml of CTAB (0.01 M) was added and the resultant solution was left under stirring overnight at 40°C. Afterward, 0.07 ml of NaOH (0.1 M) was added to the solution and left under stirring for 30 min. After this period, three injections of TEOS (0.03 ml at 20% v/v in methanol) were performed in 30 min intervals. Finally, the solution was left under stirring at 40°C for 24 h and the AuMSS nanorods were recovered by centrifugation (12,000*g* for 20 min at 25°C) and washed several times with ultrapure water.

2.2.2 | Removal of the surfactant template

The cytotoxic surfactant CTAB used in the synthesis of AuMSS nanorods was removed from the nanoparticles by adapting a solvent-based approach, previously described by Moreira and co-workers (Moreira et al., 2014). Briefly, nanoparticles were resuspended in an acid solution (HCl 7.5% v/v in EtOH), sonicated for 5 min, and centrifuged (18,000*g*, 20 min at 25°C). This step was repeated numerous times and was followed by additional washing cycles with EtOH (99.9% v/v) and ultrapure water. Finally, AuMSS nanorods were recovered by centrifugation (18,000*g* for 15 min) and resuspended in ultrapure water.

2.2.3 | Synthesis of T-PEG-CH_3 and T-GEL

The TESPIC-PEG-CH_3 (T-PEG-CH_3) and TESPIC-GEL (T-GEL) polymers were synthesized by adapting a method described by Rodrigues, Reis, et al. (2019). Briefly, 0.5 g of PEG-CH_3 polymer were dissolved in 20 ml of THF anhydrous, whereas 0.5 g of GEL were dissolved in 20 ml of THF (40% v/v). Both reactions were left at room temperature under a nitrogen atmosphere and magnetic stirring for 6 h. Next, TESPIC was added in a molar ratio of 1:1 for PEG-CH_3 and 2:1 for GEL and left under magnetic stirring for 24 h. Afterward, the T-PEG-CH_3 and T-GEL polymers were recovered by evaporation (Rotavap®R-215, Büchi), and the obtained film was resuspended with ultrapure water, sonicated, and freeze-dried.

The successful synthesis of the polymer-TESPIC derivatives was accessed using the Fourier-transform infrared (FTIR) spectroscopy.

2.2.4 | AuMSS nanorods functionalization with T-PEG-CH_3 and T-GEL

The surface functionalization of AuMSS nanorods was accomplished via condensation of the polymer silanated derivatives, T-PEG-CH_3 and T-GEL (Rodrigues, Reis, et al., 2019). First, 20 mg of AuMSS nanorods were resuspended in 40 ml of EtOH (33%, pH 4) and sonicated for 10 min. Then, T-PEG-CH_3 and T-GEL polymers were added to the AuMSS nanorods solution with a T-PEG-CH_3/T-GEL ratio of 3:1 (w/w) and left under stirring at 900 rpm for 24 h. Finally, the AuMSS/T-PEG-CH_3/T-GEL nanorods were recovered by centrifugation (8000*g*, 20 min at 25°C) and washed several times with ultrapure water to remove the unlinked polymers chains.

2.2.5 | Characterization of nanocarriers physicochemical properties

The morphology of the AuMSS and AuMSS/T-PEG-CH_3/T-GEL nanoparticles was evaluated by TEM (TEM-Hitachi-HT7700). Briefly, the samples were placed in formvar-coated copper grids and left to dry at room temperature. The TEM images were obtained at an accelerating voltage of 80 and 200 kV. Further, the silica shell thickness and nanoparticles' total size and gold core size were measured using ImageJ 2.0.0 (NIH Image). The successful purification and functionalization of AuMSS nanorods were evaluated through FTIR. The nanoformulations' FTIR spectra were obtained by using a Nicolet iS10 spectrometer with a 4 cm^{-1} spectral resolution from 600 to 4000 nm (Thermo Scientific Inc). The data acquired were analyzed in the OMNIC spectra software (Thermo Fisher Scientific). The T-PEG-CH_3 and T-GEL content on AuMSS nanorods was measured by performing a thermogravimetric analysis (TGA) of AuMSS and AuMSS/T-PEG-CH_3/T-GEL nanoparticles. For that purpose, samples were subjected to increasing temperatures up to 600°C (rate of 10°C/min under an inert atmosphere) and the nanoparticles' weight loss was recorded along the time using an SDT Q600 equipment (TA Instruments).

To confirm the success of AuMSS nanoformulations' synthesis and NIR absorption capacity a UV-Vis spectrum was acquired using a UV-Vis spectrophotometer (Thermo Scientific Evolution™ 201, Bio UV-Vis Spectrophotometer, Thermo Fisher Scientific Inc) with a wavelength range between 300 and 1100 nm at a scan rate of 300 nm/min. The zeta potential of AuMSS nanorods, AuMSS/T-PEG-CH_3/T-GEL, and AuMSS/T-PEG-CH_3/T-GEL loaded with IR780 (IR780@T-PEG-CH_3/T-GEL) was measured using a Zetasizer Nano ZS equipment (Malvern Instruments). The measurements were performed in ultrapure water at 25°C in a disposable capillary cell.

2.2.6 | The IR780 loading on AuMSS/T-PEG-CH_3/T-GEL

IR780 was loaded on AuMSS and AuMSS/T-PEG-CH_3/T-GEL nanorods by adapting an impregnation method described by Moreira et al. (2017). For that purpose, AuMSS formulations were resuspended in 5 ml of methanol containing IR780 at a concentration of 40 μg/ml. The solution was sonicated for 15 min with subsequent stirring for 48 h at room temperature. Afterward, the IR780 loaded AuMSS formulations (IR780@AuMSS and IR780@AuMSS/T-PEG-CH_3/T-GEL) were recovered by centrifugation (18,000*g* for 30 min at 4°C) and freeze-dried. The obtained supernatant was used to determine the amount of IR780 that was encapsulated in AuMSS formulations. For that purpose, the absorption of the supernatant at 780 nm was measured using a UV-Vis Spectrophotometer (Thermo Scientific Evolution™ 201 Bio-UV spectrophotometer, Thermo Fisher Scientific Inc.), and the IR780 content was determined using a calibration curve (ABS = 0.3929C + 0.0201, R^2 = 0.9978).

The encapsulation efficiency (E.E.) was calculated through Equation 1:

$$\text{E.E. (\%)} = \frac{(\text{Initial IR780 weight-IR780 weight in the supernatant})}{\text{Initial IR780 weight}} \times 100 \quad (1)$$

2.2.7 | In vitro photothermal measurements

The in vitro photothermal capacity of AuMSS formulations and free IR780 was evaluated as previously reported in the literature (Dias et al., 2016). Briefly, free IR780 (1.3 μg/ml), AuMSS, AuMSS/T-PEG-CH_3/T-GEL, and IR780@AuMSS/T-PEG-CH_3/T-GEL nanorods at a concentration of 100 μg/ml were irradiated with a NIR laser (808 nm, 1.7 W cm^{-2}). During the procedure, the variation of the solution temperature was measured every minute from 1 to 10 min of irradiation by using a thermocouple sensor with an accuracy of 0.1°C. A control group without the particles and IR780 was also irradiated and the temperature changes measured. Additionally, the photothermal capacity of AuMSS formulations and free IR780 after multiple irradiations was also measured at different points (from 1 up to 5 min). Subsequently, the photothermal conversion efficiency of AuMSS formulations and free IR780 was calculated (please see Section S1.1).

2.2.8 | Cytocompatibility assay

The biocompatibility of AuMSS and AuMSS/T-PEG-CH_3/T-GEL nanorods towards HeLa (cervical cancer cell model) and FibH (Human fibroblasts) cells was determined through the resazurin-based assay (Moreira et al., 2014). Briefly, both cells lines were seeded (10,000 cells/well) into 96-well flat-bottom culture plates and cultured with 100 μl of medium (DMEM-HG for HeLa cells and DMEM-F12 medium for FibH cells) in an incubator with a humidified atmosphere (37°C, 5% CO_2) during 24 h. Posteriorly, cells were incubated with different concentrations (25–200 μg/ml) of AuMSS formulations. After 24, 48, and 72 h, the medium was replaced with 110 μl of resazurin solution 10% (v/v) and incubated for 4 h in the dark at 37°C and 5% CO_2. After this time, the cells' viability was determined by measuring the fluorescence of the produced resorufin using a microwell plate reader (Spectramax Gemini XS, Molecular Devices LCC) at an excitation/emission wavelength of λex = 560 nm and λem = 590 nm. Cells incubated with EtOH (99.9%) and cells only incubated with culture medium were used as positive (K^+) and negative (K^-) controls, respectively.

2.2.9 | Evaluation of AuMSS nanoformulations' cellular uptake

The uptake of AuMSS and AuMSS/T-PEG-CH_3/T-GEL nanorods by HeLa or FibH cells was determined by fluorescence spectroscopy according to a method described by Moreira, Rodrigues, Reis, Costa, Ferreira, et al. (2018). Briefly, HeLa or FibH cells were seeded into 96-well flat-bottom culture plates at a density of 10,000 cells per well and cultured for 24 h, at 37°C, 5% CO_2 humidified atmosphere. After this period, the culture media was removed, and the cells were incubated with FITC stained AuMSS nanoformulations at a concentration of 100 and 200 μg/ml for 2 h. In one test group, the cells were previously treated with GEL (200 μg/ml) for 4 h. Then, the cells were washed with ice-cold Krebs Ringer Buffer (KRB) and lysed with 1% Triton X-100 in KRB for 30 min at 37°C. Cells incubated only with KRB were used as a control. Afterward, FTIC fluorescence (λex = 490 nm and λem = 520 nm), was quantified using a Spectramax Gemini XS (Molecular Devices LCC).

Additionally, the internalization of AuMSS nanoformulations by HeLa cells was confirmed by confocal laser scanning microscopy (CLSM; Gaspar et al., 2015). Briefly, HeLa cells were seeded on μ-Slide eight-well Ibidi imaging plates with a cell density of 20,000 cells per well and incubated for 24 h, at 37°C, 5% CO_2 humidified atmosphere. After this time, the medium was removed, and cells were incubated with FITC stained AuMSS nanoformulation at a concentration of 200 μg/ml. After 6 h, the cells were washed with PBS, fixed with PFA (4% w/v) for 10 min, and washed again with PBS. Then, cells were treated with Hoechst 33342® and WGA-Alexa Flour 594 for cell nucleus and cytoplasm staining, respectively. The CLSM images were obtained using a Zeiss LSM 710 Confocal microscope (Carl Zeiss SMT Inc.). The image analysis was performed in the Zeiss Zen 2010 software.

2.2.10 | Evaluation of intracellular ROS generation

The generation of intracellular ROS was assessed using the H_2DCF-DA probe, as described by Dias et al. (2016). Initially, HeLa cells were seeded in 96-well plates with a cell density of 10,000 cells per well

and cultured for 24 h, at 37°C, and 5% CO_2 humidified atmosphere. Then, cells were incubated with nanoparticles (100 and 200 μg/ml) for 4 h. Subsequently, the cell medium was removed, and 10 mM of the H_2DCF-DA solution was added in the dark (at 37°C, a humidified atmosphere with 5% CO_2). After 1 h of incubation with the H_2DCF-DA probe, the cells were washed two times with PBS and fresh medium (phenol red-free). Cells cultured only with culture medium and nonirradiated cells cultured with nanoparticles (100 μg/ml) were used as control groups. Then, the cells were irradiated with a NIR laser (808 nm, 1.7 W cm^{-2}) for 5 min, washed with ice-cold KBR, and lysed with 1% Triton X-100 in KRB for 30 min at 37°C. Finally, H_2DCF-DA fluorescence (λex = 488 nm and λem = 540 nm) was quantified using a Spectramax Gemini XS plate reader (Molecular Devices LLC).

2.2.11 | Evaluation of AuMSS nanoformulations phototherapeutic effect

Characterization of the AuMSS in vitro cytotoxic activity

The cytotoxic effect of free IR780 and AuMSS nanoformulations (AuMSS, AuMSS/T-PEG-CH_3/T-GEL, and IR780@AuMSS/T-PEG-CH_3/T-GEL) was determined in vitro using the resazurin assay (Moreira, Rodrigues, Reis, Costa, Ferreira, et al., 2018). For that purpose, 10,000 HeLa cells were seeded in 96-well plates and cultured for 24 h. Afterward, the cells were incubated with free IR780 (0.65, 1.3, and 2.6 μg/ml) or AuMSS nanoformulations at different concentrations (50, 100, and 200 μg/ml) for 24 h. Then, the cells were irradiated with a NIR laser (808 nm, 1.7 W cm^{-2}) for 5 min. Nonirradiated cells were used as control. After 24 h, the cells' viability was assessed using the resazurin method as described above. Cells incubated with EtOH (99.9%) and cells only incubated with culture medium were used as K^+ and negative K^- controls, respectively.

Live/death assay

The phototherapeutic effect mediated by AuMSS, AuMSS/T-PEG-CH_3/T-GEL, IR780@AuMSS/T-PEG-CH_3/T-GEL nanorods, and free IR780 was also evaluated by fluorescence microscopy through the Live/Dead assay (Invitrogen, Life Technologies). For that purpose, HeLa cells were seeded on μ-Slide eight-well Ibidi imaging plates (Ibidi GmbH), and incubated at 37°C in a humidified atmosphere (5% CO_2). After 48 h, HeLa cells were treated with AuMSS nanoformulations (100 μg/ml) or free IR780 (1.3 μg/ml) for 24 h and irradiated with a NIR laser (808 nm, 1.7 W cm^{-2}) for 5 min. Afterward, cells were stained with Calcein AM and PI to allow the visualization of live and dead cells, respectively. Finally, the live/death images were obtained by CLSM (Zeiss LSM 710, Carl Zeiss).

2.2.12 | Statistical analysis

Data are presented as the mean ± standard deviation (s.d.). The statistical analysis of experiments with two groups was performed with the unpaired Student's *t*-test. One-way analysis of variance (ANOVA) with the Student–Newman–Keuls posttest was used for multiple groups comparison. A *p*-value lower than 0.05 was statistically significant. Statistical analysis was performed using GraphPad Prism v.6.0 software (Trial version, GraphPad Software).

3 | RESULTS AND DISCUSSION

3.1 | Synthesis and characterization of T-PEG-CH_3 and T-GEL polymers

The PEG-CH_3 and GEL polymers were modified with TESPIC (T-PEG-CH_3 and T-GEL silane derivatives) through a hydrogen-transfer nucleophilic addition reaction to enable their posterior chemical grafting in AuMSS surface (Figure S1). The modification of GEL and PEG-CH_3 with TESPIC was confirmed through FTIR analysis. The FTIR spectra of GEL and T-GEL show the characteristic peaks of GEL at 3288 cm^{-1}, corresponding to the N-H vibrations, and at 1680–1640 cm^{-1} region attributed to the strong C=O stretching of amide II (Haroun & El Toumy, 2010). After modification with TESPIC, the T-GEL spectrum showed some changes at the 1000–1100 cm^{-1} region due to the absorption band of the Si–O–C bonds. Otherwise, the T-PEG-CH_3 shows both the PEG-CH_3 characteristic peaks at 2800–2900 cm^{-1} (C-H stretching) and the peaks corresponding to the C=O stretching of amide II (1680–1640 cm^{-1}) bond resulting from the TESPIC linkage (Figure S2; Jacinto et al., 2020).

3.2 | Synthesis and characterization of AuMSS nanorods

The synthesis of AuMSS nanorods was performed using a seed-mediated methodology already described in the literature (Gorelikov & Matsuura, 2008; Nikoobakht & El-Sayed, 2003) The synthesis method is divided into three main steps: (i) production of small gold spheres (seeds), (ii) seed growth forming the gold nanorods, (iii) and the coating with a mesoporous silica shell, using CTAB as a template to promote the formation of the mesopores. The successful synthesis of the AuMSS nanorods and their core-shell organization was confirmed by TEM images (Figure 1a). The analysis of TEM images demonstrates the presence of gold nanorods coated with a mesoporous silica shell. Further, the ImageJ measurements show that the gold core had a mean length and width of 53 ± 11 and 19 ± 4 nm, respectively, corresponding to an A.R. of 2.8. Additionally, the AuMSS nanorods present a mesoporous silica layer with 30 nm of thickness, which results in nanoparticles with a total length and width of 96 ± 15 and 66 ± 14 nm, respectively (Figure 1b). After the AuMSS nanorods functionalization with T-PEG-CH_3 and T-GEL polymers, the TEM images analysis does not show any significant changes in overall nanoparticles size (*L*: 84 ± 14 nm and *W*: 52 ± 10 nm, Figure 1d). Thus, the overall size of AuMSS formulations allows them to take advantage of the enhanced permeability and retention effect, which

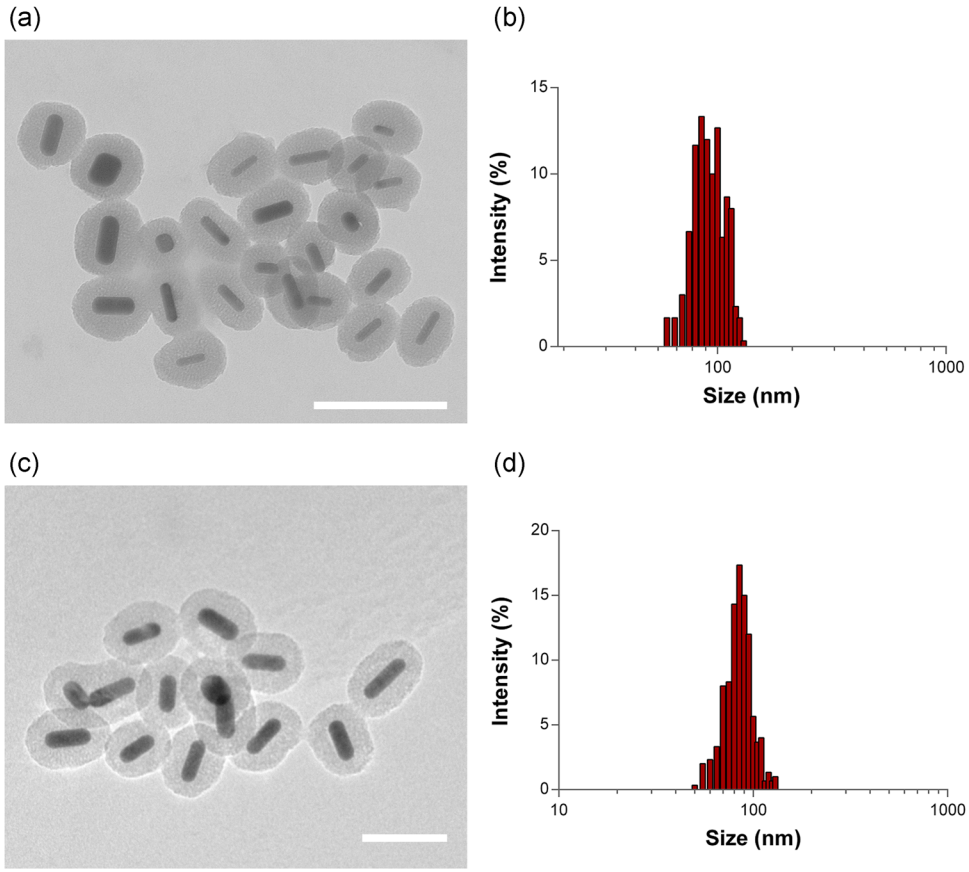

FIGURE 1 Structural analysis of AuMSS nanorods. TEM images of AuMSS (a) and AuMSS/T-PEG-CH_3/T-GEL (c) nanorods. Scale bar corresponds to 200 nm (a) and 100 nm (c). Size distribution (length and width included) of AuMSS (b) and AuMSS/T-PEG-CH_3/T-GEL (d) nanorods, $n = 300$

consequently enable their passive accumulation in the tumor tissue (de Melo-Diogo et al., 2017).

The successful removal of the CTAB and the formation of the mesoporous silica shell were evaluated by FTIR analysis (Figure 2a). CTAB possesses two characteristic peaks, 2850–2950 cm^{-1} (corresponding to the C-H vibration), and 1450–1500 cm^{-1} (corresponding to the CH_3-N^+ deformation; Dias et al., 2016). Therefore, the absence of these two characteristic bands in the AuMSS nanorods FTIR spectrum confirms the complete removal of the cytotoxic CTAB molecules. Additionally, it is also possible to observe the characteristic peaks of the mesoporous silica shell in the 750–1150 cm^{-1}, which correspond to Si-O-Si and Si-OH vibrations (Moreira et al., 2014).

3.3 | Functionalization of the AuMSS nanorods

The immobilization of T-PEG-CH_3 and T-GEL on the surface of the AuMSS nanorods was achieved by exploring the condensation of the silane-modified polymers with the Si-OH groups that are present on the silica surface, originating the AuMSS/T-PEG-CH_3/T-GEL nanorods. The functionalization of AuMSS nanorods was evaluated by recording the changes in the nanoparticles' zeta potential. The AuMSS nanorods presented a negative surface charge, −23 mV, due to the silanol groups present on the mesoporous silica surface (Figure 2b). The immobilization of T-PEG-CH_3 and T-GEL resulted in the neutralization of the AuMSS surface charge to −7.46 mV. Such can have a great impact on the nanorods' performance since neutral surface charges (±10 mV) are often considered ideal for biological applications due to the reduced RES recognition and improved blood circulation time (Fröhlich, 2012).

Additionally, the functionalization of AuMSS nanoparticles was also confirmed through FTIR analysis (Figure 2a). The AuMSS/T-PEG-CH_3/T-GEL presented the characteristic peaks of mesoporous silica in the 750–1100 cm^{-1} region, as well as the PEG-CH_3 C-H stretching at 2900 cm^{-1} and the GEL C=O stretching at 1650 cm^{-1}. Further, the polymer content on AuMSS/T-PEG-CH_3/T-GEL nanoparticles was determined by TGA analysis. In Figure 2c, it is possible to observe that bare AuMSS nanorods present only 4% of weight loss, which can be attributed to the evaporation of water molecules in the interior of the mesopores and the loss of the hydroxyl groups present on nanoparticles' surface. Otherwise, the AuMSS/T-PEG-CH_3/T-GEL presented a weight loss of 20% due to the pyrolysis of the polymers. Overall, the presented results corroborate the successful immobilization of GEL and PEG on the surface of the AuMSS nanorods.

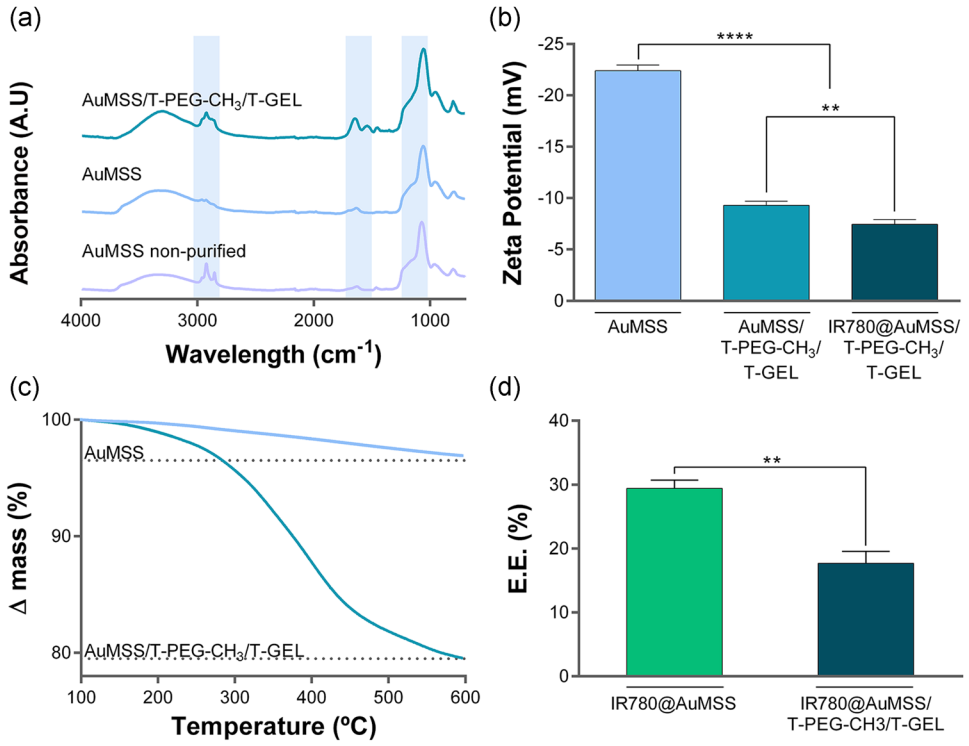

FIGURE 2 Physicochemical characterization of AuMSS formulations. (a) FTIR spectra of non-purified AuMSS, AuMSS, and AuMSS/T-PEG-CH_3/T-GEL nanorods. (b) Surface charge of AuMSS, AuMSS/T-PEG-CH_3/T-GEL, and IR780@AuMSS/T-PEG-CH_3/T-GEL. Data are presented as mean ± s.d., $^{**}p < 0.01$, $^{****}p < 0.0001$; $n = 3$. (c) TGA analysis of AuMSS and AuMSS/T-PEG-CH_3/T-GEL nanoparticles. (d) IR780 E.E. on AuMSS and AuMSS/T-PEG-CH_3/T-GEL nanoparticles. Data are presented as mean ± s.d., $^{**}p < 0.01$; $n = 3$. TGA, thermogravimetric analysis

3.4 | Evaluation of the IR780 loading

The AuMSS and AuMSS/T-PEG-CH_3/T-GEL nanorods' ability to encapsulate IR780 was characterized by measuring the E.E. The encapsulation of the IR780 was performed by resuspending AuMSS and AuMSS/T-PEG-CH_3/T-GEL nanorods in the IR780 solution for 48 h. The results show that AuMSS and AuMSS/T-PEG-CH_3/T-GEL nanorods presented an E.E of 29.4% and 17.7%, respectively (Figure 2d). As expected, the results demonstrate that the AuMSS functionalization with T-PEG-CH_3 and T-GEL decreases the E.E. of the IR780, which can be attributed to a repulsion phenomenon (negatively charged polymers and IR780 molecules) and/or the blockage of AuMSS pores by the polymers. Moreover, such behavior is coherent with other reports available in the literature where the introduction of surface functionalization hinders the drug loading capacity of mesoporous silica-based nanomaterials (Rodrigues, Jacinto, et al., 2019; Shen et al., 2013).

3.5 | In vitro evaluation of the photothermal capacity of AuMSS nanoformulations

The AuMSS, AuMSS/T-PEG-CH_3/T-GEL, and IR780@AuMSS/T-PEG-CH_3/T-GEL nanoformulations ability to be applied as photothermal agents was initially verified through UV-vis analysis (Figure S3). As expected, free IR780 presented a well-defined absorption peak in the NIR region at 780 nm. Otherwise, the UV-vis spectra of AuMSS nanorods show two absorption bands at 520 nm and 750 nm (i.e., NIR region), which correspond to the characteristic transversal and longitudinal plasmon resonances of gold nanorods. The strong absorption peak at 750 nm, NIR-I region of the spectra, supports the application of AuMSS nanorods as photothermal agents. Moreover, the functionalization of the AuMSS nanorods with PEG-CH_3 and GEL did not induce any significant changes in the nanoparticles' absorption spectrum. Further, apart from the two absorption bands at 520 nm and 750 nm, the IR780@AuMSS/T-PEG-CH_3/T-GEL nanorods also presented a small deformation in the absorption spectra at ≈780 nm. Such corroborates the previous results demonstrating the successful loading of IR780 in the AuMSS nanorods.

Then, the photothermal capacity of the free IR780 and the AuMSS nanoformulations was evaluated by measuring the temperatures changes when exposed to a NIR laser (808 nm, 1.7 W cm^{-2}) for 1 to 10 min (Figure 3a). It was possible to observe that both AuMSS nanoformulations can mediate a gradual temperature increase during the 10 min of irradiation. At a concentration of 100 μg/ml both AuMSS and AuMSS/T-PEG-CH_3/T-GEL mediated a ≈35°C temperature increase, contrasting with the 3–4°C obtained with the free IR780 (1.3 μg/ml—a concentration equivalent to the IR780@AuMSS/T-PEG-CH_3/T-GEL). Otherwise, the IR780@AuMSS/T-PEG-CH_3/T-GEL nanorods presented a higher photothermal capacity, reaching a ΔT of ≈40°C after 6 min of irradiation. Nevertheless, from the 8 min of irradiation onward, the temperature of

the medium started to decrease to a final ΔT of ≈37°C. This photothermal behavior can be explained by the photodegradation of IR780 upon continuous irradiation with NIR light (Guo et al., 2016; Leitão et al., 2020; Wang et al., 2016). Alves and colleagues also observed that the temperature increase mediated by IR780-loaded hyaluronic acid-based nanoparticles peaks at ≈10°C after 1 min of irradiation and starts to decrease to 4°C in the following 4 min (Alves et al., 2019). To confirm the obtained results, the photothermal stability of IR780@AuMSS/T-PEG-CH_3/T-GEL nanoparticles and free IR780 were evaluated by performing multiple irradiation cycles (Figure 3b,c). After multiple NIR irradiations, free IR780 showed a decrease in the maximum ΔT achieved, while IR780@AuMSS/T-PEG-CH_3/T-GEL maintained their photothermal profile, demonstrating the photothermal stability of the gold core. This enhanced photothermal stability can be explored for improving the therapeutic efficacy by performing multiple cycles of irradiation in the tumor tissue.

Finally, the UV-vis and in vitro PTT results were used to calculate the photothermal conversion efficiency (please see Section S1.1) of the different AuMSS nanoformulations. The obtained results demonstrate that the encapsulation of IR780 improves the photothermal performance of AuMSS nanoparticles, the calculated photothermal conversion efficiency for AuMSS, AuMSS/T-PEG-CH_3/T-GEL, and IR780@AuMSS/T-PEG-CH_3/T-GEL was 88.1%, 88.3%, and 96.1%, respectively (Figure 3d). Such data are in agreement with the superior photothermal capacity demonstrated by IR780@AuMSS/T-PEG-CH_3/T-GEL and can be particularly advantageous for achieving superior heat generation in cases of sub-optimal laser irradiation (e.g., deep-seated tumors).

3.6 | Characterization of the AuMSS nanorods biocompatibility

The cytocompatibility of AuMSS and AuMSS/T-PEG-CH_3/T-GEL nanorods was assessed both on HeLa and FibH cells through the resazurin assay. For that purpose, different concentrations of AuMSS nanoformulations (25–200 μg/ml) were incubated with the cells for 24, 48, and 72 h. Therefore, Figure S4 demonstrates that both AuMSS and AuMSS/T-PEG-CH_3/T-GEL nanorods are biocompatible in all concentrations tested. These results are in agreement with the results described in the literature for AuMSS nanorods as well as with the safety profiles of GEL and PEG-CH_3 (FDA-approved polymers for biomedical applications; Dias et al., 2016; Laha et al., 2016).

3.7 | AuMSS nanorods uptake by HeLa and FibH cells

The nanoparticles uptake by cancer cells is one of the last barriers that nanoparticles have to surpass to induce their therapeutic effect. The nanoparticles' modification with agents that possess the ability to

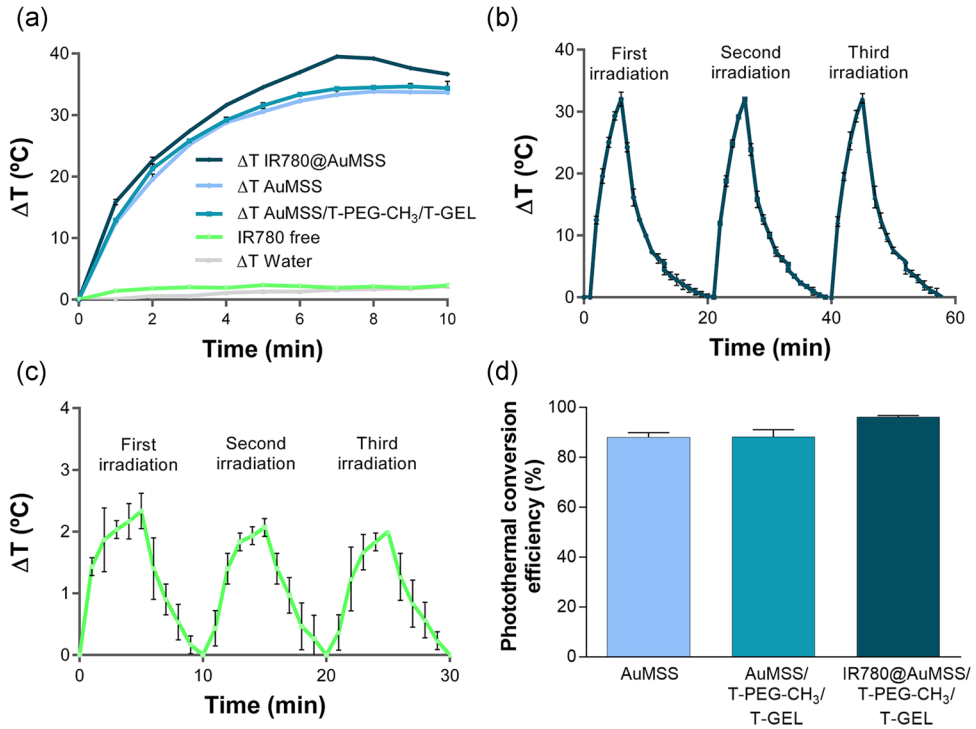

FIGURE 3 Characterization of the PTT capacity of AuMSS nanoformulations and free IR780. (a) Temperature variation curve of AuMSS nanoformulations and free IR780 upon irradiation with NIR laser (808 nm, 1.7 W cm^{-2}, 10 min). Temperature variation curve of (b) IR780@AuMSS/T-PEG-CH_3/T-GEL nanoparticles and (c) free IR780 after multiple irradiations with NIR laser (808 nm, 1.7 W cm^{-2}, 5 min). (d) Analysis of the photothermal conversion efficiency of AuMSS, AuMSS/T-PEG-CH_3/T-GEL, and IR780@AuMSS/T-PEG-CH_3/T-GEL. Data are presented as mean ± s.d., $n = 3$. PTT, photothermal therapy

actively target cancer cells is one of the main approaches to improve the selectivity and the nanoparticles' uptake by cancer cells. For that purpose, the uptake of AuMSS and AuMSS/T-PEG-CH_3/T-GEL nanorods was evaluated both in HeLa and FibH cells using fluorescence spectroscopy and CLSM (Figure 4). Afterward, the GEL targeting capacity was evaluated by measuring the fluorescence of the FITC-labeled AuMSS nanoformulations in HeLa (high $\alpha v\beta_3$ expression) and FibH (low $\alpha v\beta_3$ expression) cells through fluorescence spectroscopy (Figure 4a,b). The obtained results demonstrated that the HeLa cells treated with FITC-stained AuMSS/T-PEG-CH_3/T-GEL nanorods presented a ≈1.7-times higher fluorescence intensity than those treated with AuMSS. Further, no significant differences were observed in the uptake of AuMSS formulations by FibH cells. Such results indicated that the increased uptake of AuMSS/T-PEG-CH_3/T-GEL nanorods in HeLa could be mediated by the interaction of RGD sequences available in GEL with the overexpressed $\alpha v\beta_3$ integrins. With that in mind, both HeLa and FibH were treated with free GEL for 4 h before the incubation with AuMSS nanoformulation. Such resulted in the reduction of the AuMSS/T-PEG-CH_3/T-GEL nanorods uptake in HeLa cells to values similar to those of AuMSS nanorods. Therefore, this experiment demonstrated that the introduction of GEL in the AuMSS nanorods confer to the nanoparticles a preferential uptake in cancer cells overexpressing the $\alpha v\beta_3$ integrins. Such behavior is in accordance with the data available in the literature, where the functionalization of the nanoparticles with RGD sequences increased their cellular uptake by cancer cells overexpressing the $\alpha v\beta_3$ integrins (Li et al., 2017; J. Yang et al., 2015; Zhou et al., 2017). Additionally, the uptake of AuMSS

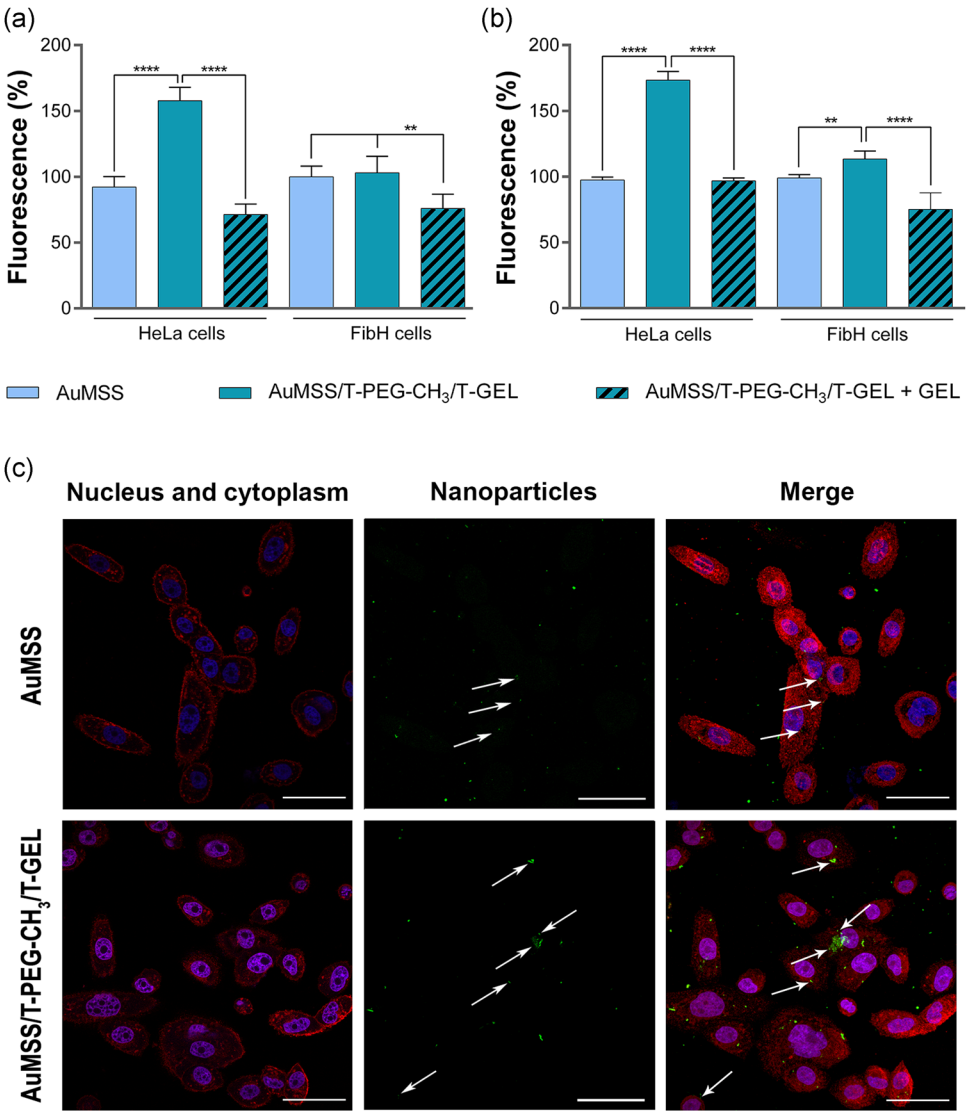

FIGURE 4 Analysis of the AuMSS nanoformulations uptake by HeLa and FibH cells. Fluorescence spectroscopy analysis of the FibH and HeLa cells uptake of AuMSS nanoformulations at 100 μg/ml (a) and 200 μg/ml (b). Data are presented as mean ± s.d., $^{**}p < 0.01$, $^{****}p < 0.0001$; $n = 5$. (c) Representative confocal microscopy images of the internalization of AuMSS nanoformulations by HeLa cells after 6 h of incubation. The white arrows are pointing to the internalized nanoparticles. The scale bar corresponds to 50 μm. Blue channel: Hoechst 33342® stained cell nucleus; red channel: WGA-Alexa Fluor® 594 stained cell cytoplasm; green channel: FITC labeled nanoparticles

nanoformulation by HeLa cells was also confirmed by CLSM. Further, in confocal images (Figure 4c), it is possible to co-localize the FITC fluorescence (i.e., stained nanoparticles) with the cell cytoplasm, highlighted with the white arrows, confirming that both the AuMSS and AuMSS/T-PEG-CH_3/T-GEL can be internalized by HeLa cells.

3.8 | Evaluation of intracellular ROS generation in HeLa cells

The intracellular generation of ROS by HeLa cells treated with free IR780, AuMSS, AuMSS/T-PEG-CH_3/T-GEL, or IR780@AuMSS/T-PEG-CH_3/T-GEL, in the presence or absence of NIR irradiation, was assessed using the H_2DCF-DA probe (Dias et al., 2016). The obtained results revealed that all the nanoformulations present an increased ROS generation upon NIR light irradiation (Figure 5b). Additionally, it is possible to observe that the group treated with the IR780@AuMSS/T-PEG-CH_3/T-GEL presents a two times higher ROS generation when compared to the other AuMSS formulations. Such an increase in the generation of ROS can be explained by the encapsulation of IR780, protecting it from premature photodegradation, and its capacity to generate ROS in response to NIR laser irradiation. Moreover, it is worth noticing that this light-triggered effect and the short lifetime of ROS should allow the confinement of its action to the tumor site, with minimal side-effect on the surrounding area.

3.9 | Characterization of the AuMSS nanoformulations' photothermal cytotoxic activity

The anticancer potential of AuMSS nanoformulations as well as its capacity to combine PTT and PDT was evaluated in HeLa cells. For that purpose, HeLa cells were incubated with different concentrations of free IR780 (0.65, 1.3, and 2.6 μg/ml, equivalent to that found in the nanoparticles) and AuMSS nanoformulations (50, 100, and 200 μg/ml) for 24 h, and subjected to irradiation with a NIR laser (808 nm, 1.7 W cm^{-2}; for 5 min). In Figure 6c, it can be observed that all AuMSS nanoformulations induced a decrease in the cancer cells' viability to values inferior to 5% when the concentration was superior to 100 μg/ml. Moreover, at these concentration values, no significant differences were observed between the different AuMSS nanoformulations. Such results are in accordance with the previously described photothermal data, where the AuMSS nanoformulations can mediate a temperature increase superior to 30°C upon NIR laser irradiation. As described in the literature, temperatures higher than 45°C led to the elimination of cancer cells by promoting DNA damages, protein denaturation, and the destruction of the cell membrane. However, at the lowest concentration tested (50 μg/ml), the group treated with IR780@AuMSS/T-PEG-CH_3/T-GEL nanorods presented the lowest cell viability (≈50%), followed by AuMSS/T-PEG-CH_3/T-GEL, AuMSS nanorods, and IR780. This enhanced antitumoral capacity of IR780@AuMSS/T-PEG-CH_3/T-GEL nanorods can be explained by the increased photothermal capacity as well as the combination of PTT and PDT. Additionally, the results also show an improved antitumoral capacity of AuMSS/T-PEG-CH_3/T-GEL when compared with AuMSS nanorods. Such difference demonstrates one more time the importance of GEL-mediated active targeting towards HeLa cancer cells, which increases the nanoparticle uptake by the cancer cells maximizing the therapeutic effect.

Further, the photothermal effect mediated by the AuMSS/T-PEG-CH_3/T-GEL and IR780@AuMSS/T-PEG-CH_3/T-GEL on HeLa cells was also confirmed by the Live/Dead assays. The CLSM images (Figure 6a,b) showed the presence of a zone with a high number of dead cells (red fluorescence) within the area irradiated with the NIR laser. Such confirm that the AuMSS/T-PEG-CH_3/T-GEL and IR780@AuMSS/T-PEG-CH_3/T-GEL nanorods can be activated by the irradiation of a NIR laser. Therefore, this on-demand and

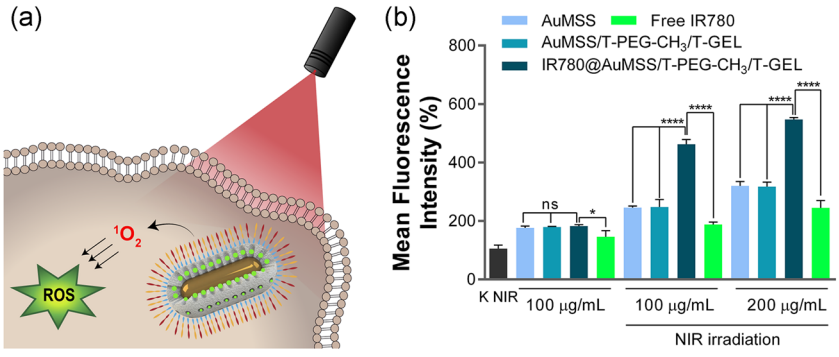

FIGURE 5 Analysis of the intracellular generation of ROS in HeLa cancer cells. (a) Schematic representation of the experiment. (b) Evaluation of the intracellular generation of ROS in HeLa cancer cells, fluorescence was normalized towards the K NIR group. K NIR: HeLa cells incubated with medium and irradiated with NIR laser (808 nm, 1.7 W cm^{-2}, 5 min). Data are presented as mean ± s.d., $^*p < 0.05$, $^{****}p < 0.0001$; $n = 5$; ns, nonsignificant; ROS, reactive oxygen species

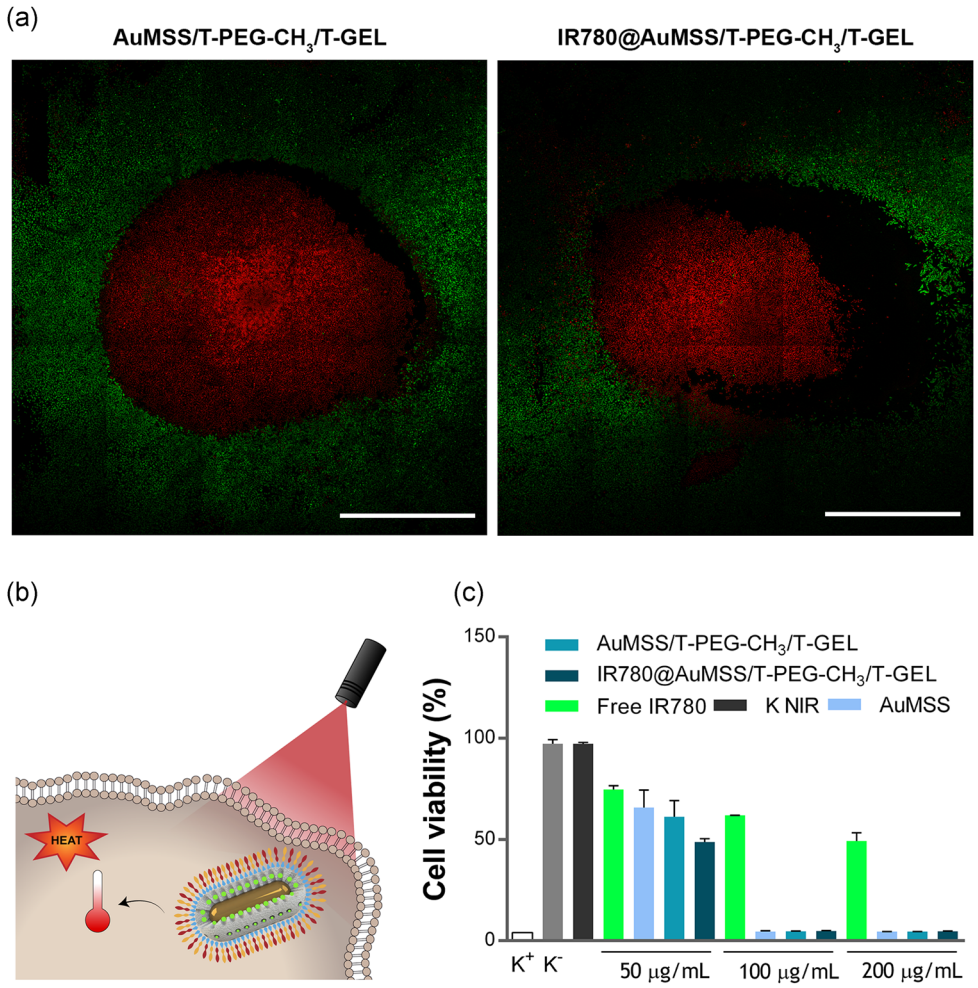

FIGURE 6 Analysis of the photothermal cytotoxic effect of AuMSS nanoformulations' in HeLa cancer cells. (a) Live/Dead CLSM images of the HeLa cells incubated with AuMSS nanoformulations at a concentration of 100 μg/ml and irradiated with a NIR laser (808 nm, 1.7 W cm^{-2}, 5 min). Green channel: Calcein stained cells; Red channel: PI stained cells. Scale bar: 200 μm. (b) Schematic representation of the AuMSS nanoformulations' cytotoxic activity upon NIR irradiation. (c) Analysis of the HeLa cells viability in response to the treatment with free IR780 or AuMSS nanoformulations. K^+: cells treated with EtOH. K^-: cells without nanoparticles incubation. CLSM, confocal laser scanning microscopy

laser-dependent behavior can be explored to confine the treatment to the target tumoral tissue. Moreover, the combination of AuMSS/T-PEG-CH_3/T-GEL and IR780 proved to be more effective than the therapeutic application of AuMSS/T-PEG-CH_3/T-GEL nanoparticles alone.

4 | CONCLUSION

The application of nanoparticles capable of mediating a photothermal effect has been gaining great attention by researchers. Among the different nanoparticles applied in PTT, rod-shaped AuMSS nanoparticles present excellent physicochemical and biological properties that make them promising nanoplatforms for cancer therapy. However, it is crucial to improve their blood circulation time, cancer cells' specificity, and photothermal performance. The obtained results demonstrate that the functionalization of AuMSS nanorods did not impact their overall size and PTT capacity. Otherwise, the polymers grafting on the AuMSS nanorods induced the neutralization of the surface, which can enhance the nanoparticle circulation in the bloodstream. Additionally, the loading of IR780 in AuMSS/T-PEG-CH_3/T-GEL resulted in an increased photothermal capacity (maximum temperature of ≈40°C). Additionally, the in vitro assays performed in the 2D cell culture models showed that all AuMSS nanoformulations were biocompatible and the functionalization with GEL increased the nanoparticles' internalization by the HeLa cancer cells in a process mediated by the $\alpha v\beta_3$ integrins. Finally, the IR780@AuMSS/T-PEG-CH_3/T-GEL nanorods presented an enhanced cytotoxic effect towards HeLa cancer cells due to the combination of the increased PTT capacity and PDT. Overall, the attained data support the application of AuMSS-based nanomaterials in cancer therapy. Additionally, the loading of a photothermal agent, that is, IR780, was a straightforward strategy for increasing the light-to-heat conversion efficiency of the nanomaterials, contrasting with the

laborious and complicated synthesis optimizations. Such can be pursued in future works to fast-track the translation of photothermal gold-based nanomaterials to the clinic addressing some suboptimal photothermal performances related to the radiation-mediated gold reshaping/degradation. In the future, in vivo assays will be performed to explore the IR780@AuMSS/T-PEG-CH_3/T-GEL potential to act as a targeted multifunctional nanosystem that can simultaneously perform PTT and PDT. Besides the encapsulation of IR780, the inclusion of the silica shell could also be explored to allow the simultaneous loading of chemotherapeutic drugs further enhancing the therapeutic potency of the AuMSS nanorods.

ACKNOWLEDGMENTS

This study was financed by the Foundation for Science and Technology (FCT), through funds from the State Budget, and by the European Regional Development Fund (ERDF), under the Portugal 2020 Program, through the Regional Operational Program of the Center (Centro2020), through the Project with the reference UIDB/00709/2020. The funding from CENTRO-01-0145-FEDER-028989 and POCI-01-0145-FEDER-031462 are also acknowledged. Carolina F. Rodrigues acknowledges for her PhD fellowship from FCT (SFRH/BD/144680/2019). The funders had no role in the decision to publish or in the preparation of the manuscript. Duarte de Melo-Diogo acknowledges CENTRO-01-0145-FEDER-028989 for the funding given in the form of a research contract.

CONFLICT OF INTERESTS

The authors declare that there are no conflict of interests.

DATA AVAILABILITY STATEMENT

The data that support the findings of this study are available from the corresponding author upon reasonable request.

ORCID

Ariana S. C. Gonçalves https://orcid.org/0000-0001-7408-1331
Carolina F. Rodrigues https://orcid.org/0000-0002-5493-8331
Natanael Fernandes https://orcid.org/0000-0002-7737-9288
Duarte de Melo-Diogo https://orcid.org/0000-0001-9984-3603
Paula Ferreira https://orcid.org/0000-0003-3393-4427
André F. Moreira https://orcid.org/0000-0002-0604-2506
Ilídio J. Correia http://orcid.org/0000-0003-1613-9675

REFERENCES

Alves, C. G., de Melo-Diogo, D., Lima-Sousa, R., Costa, E. C., & Correia, I. J. (2019). Hyaluronic acid functionalized nanoparticles loaded with IR780 and DOX for cancer chemo-photothermal therapy. *European Journal of Pharmaceutics and Biopharmaceutics*, *137*, 86–94.

Alves, C. G., Lima-Sousa, R., de Melo-Diogo, D., Louro, R. O., & Correia, I. J. (2018). IR780 based nanomaterials for cancer imaging and photothermal, photodynamic and combinatorial therapies. *International Journal of Pharmaceutics*, *542*(1–2), 164–175.

Danhier, F., Le Breton, A., & Préat, V. R. (2012). RGD-based strategies to target alpha (v) beta (3) integrin in cancer therapy and diagnosis. *Molecular Pharmaceutics*, *9*(11), 2961–2973.

Davidenko, N., Schuster, C. F., Bax, D. V., Farndale, R. W., Hamaia, S., Best, S. M., & Cameron, R. E. (2016). Evaluation of cell binding to collagen and gelatin: a study of the effect of 2D and 3D architecture and surface chemistry. *Journal of Materials Science: Materials in Medicine*, *27*(10), 1–14.

de Melo-Diogo, D., Lima-Sousa, R., Alves, C. G., & Correia, I. J. (2019). Graphene family nanomaterials for application in cancer combination photothermal therapy. *Biomaterials Science*, *7*(9), 3534–3551.

de Melo-Diogo, D., Pais-Silva, C., Dias, D. R., Moreira, A. F., & Correia, I. J. (2017). Strategies to improve cancer photothermal therapy mediated by nanomaterials. *Advanced Healthcare Materials*, *6*(10), 1700073.

Dias, D. R., Moreira, A. F., & Correia, I. J. (2016). The effect of the shape of gold core–mesoporous silica shell nanoparticles on the cellular behavior and tumor spheroid penetration. *Journal of Materials Chemistry B*, *4*(47), 7630–7640.

Fernandes, N., Rodrigues, C. F., Moreira, A. F., & Correia, I. J. (2020). Overview of the application of inorganic nanomaterials in cancer photothermal therapy. *Biomaterials Science*, *8*(11), 2990–3020.

Fox, M. E., Szoka, F. C., & Fréchet, J. M. (2009). Soluble polymer carriers for the treatment of cancer: The importance of molecular architecture. *Accounts of Chemical Research*, *42*(8), 1141–1151.

Fröhlich, E. (2012). The role of surface charge in cellular uptake and cytotoxicity of medical nanoparticles. *International Journal of Nanomedicine*, *7*, 5577.

Gaspar, V. M., Moreira, A. F., Costa, E. C., Queiroz, J. A., Sousa, F., Pichon, C., & Correia, I. J. (2015). Gas-generating TPGS-PLGA microspheres loaded with nanoparticles (NIMPS) for co-delivery of minicircle DNA and anti-tumoral drugs. *Colloids and Surfaces B: Biointerfaces*, *134*, 287–294.

Gómez-Guillén, M., Giménez, B., López-Caballero, M. A., & Montero, M. (2011). Functional and bioactive properties of collagen and gelatin from alternative sources: A review. *Food Hydrocolloids*, *25*(8), 1813–1827.

Gonçalves, A. S., Rodrigues, C. F., Moreira, A. F., & Correia, I. J. (2020). Strategies to improve the photothermal capacity of gold-based nanomedicines. *Acta Biomaterialia*, *116*, 105–137.

Gorelikov, I., & Matsuura, N. (2008). Single-step coating of mesoporous silica on cetyltrimethyl ammonium bromide-capped nanoparticles. *Nano Letters*, *8*(1), 369–373.

Guo, F., Yu, M., Wang, J., Tan, F., & Li, N. (2016). The mitochondria-targeted and IR780-regulated theranosomes for imaging and enhanced photodynamic/photothermal therapy. *RSC Advances*, *6*(14), 11070–11076.

Haroun, A., & El Toumy, S. (2010). Effect of natural polyphenols on physicochemical properties of crosslinked gelatin-based polymeric biocomposite. *Journal of Applied Polymer Science*, *116*(5), 2825–2832.

Harris, J. M., & Chess, R. B. (2003). Effect of pegylation on pharmaceuticals. *Nature Reviews Drug Discovery*, *2*(3), 214–221.

Hoch, E., Schuh, C., Hirth, T., Tovar, G. E., & Borchers, K. (2012). Stiff gelatin hydrogels can be photo-chemically synthesized from low viscous gelatin solutions using molecularly functionalized gelatin with a high degree of methacrylation. *Journal of Materials Science: Materials in Medicine*, *23*(11), 2607–2617.

Hoque, M. E., Nuge, T., Yeow, T. K., Nordin, N., & Prasad, R. (2015). Gelatin based scaffolds for tissue engineering—A review. *Polymers Research Journal*, *9*(1), 15.

Huang, X., Jain, P. K., El-Sayed, I. H., & El-Sayed, M. A. (2008). Plasmonic photothermal therapy (PPTT) using gold nanoparticles. *Lasers in Medical Science*, *23*(3), 217–228.

Hussain, Z., Khan, S., Imran, M., Sohail, M., Shah, S. W. A., & de Matas, M. (2019). PEGylation: A promising strategy to overcome challenges to cancer-targeted nanomedicines: A review of challenges to clinical

transition and promising resolution. *Drug Delivery and Translational Research*, *9*(3), 721–734.

Jacinto, T. A., Rodrigues, C. F., Moreira, A. F., Miguel, S. P., Costa, E. C., Ferreira, P., & Correia, I. J. (2020). Hyaluronic acid and vitamin E polyethylene glycol succinate functionalized gold-core silica shell nanorods for cancer targeted photothermal therapy. *Colloids and Surfaces B: Biointerfaces*, *188*, 110778.

Jiang, X., Du, B., Huang, Y., Yu, M., & Zheng, J. (2020). Cancer photothermal therapy with ICG-conjugated gold nanoclusters. *Bioconjugate Chemistry*, *31*(5), 1522–1528.

Laha, A., Majumdar, S., & Sharma, C. S. (2016). Controlled drug release formulation by sequential crosslinking of multilayered electrospun gelatin nanofiber mat. *MRS Advances*, *1*(29), 2107–2113.

Leitão, M. M., de Melo-Diogo, D., Alves, C. G., Lima-Sousa, R., & Correia, I. J. (2020). Prototypic heptamethine cyanine incorporating nanomaterials for cancer phototheragnostic. *Advanced Healthcare Materials*, *9*(6), 1901665.

Li, X., Xing, L., Hu, Y., Xiong, Z., Wang, R., Xu, X., Du, L., Shen, M., & Shi, X. (2017). An RGD-modified hollow silica@ Au core/shell nanoplatform for tumor combination therapy. *Acta Biomaterialia*, *62*, 273–283.

Liu, J., Detrembleur, C., De Pauw-Gillet, M. C., Mornet, S., Jérôme, C., & Duguet, E. (2015). Gold nanorods coated with mesoporous silica shell as drug delivery system for remote near infrared light-activated release and potential phototherapy. *Small*, *11*(19), 2323–2332.

Moreira, A. F., Dias, D. R., & Correia, I. J. (2016). Stimuli-responsive mesoporous silica nanoparticles for cancer therapy: A review. *Microporous and Mesoporous Materials*, *236*, 141–157.

Moreira, A. F., Dias, D. R., Costa, E. C., & Correia, I. J. (2017). Thermo-and pH-responsive nano-in-micro particles for combinatorial drug delivery to cancer cells. *European Journal of Pharmaceutical Sciences*, *104*, 42–51.

Moreira, A. F., Gaspar, V. M., Costa, E. C., de Melo-Diogo, D., Machado, P., Paquete, C. M., & Correia, I. J. (2014). Preparation of end-capped pH-sensitive mesoporous silica nanocarriers for on-demand drug delivery. *European Journal of Pharmaceutics and Biopharmaceutics*, *88*(3), 1012–1025.

Moreira, A. F., Rodrigues, C. F., Reis, C. A., Costa, E. C., & Correia, I. J. (2018). Gold-core silica shell nanoparticles application in imaging and therapy: A review. *Microporous and Mesoporous Materials*, *270*, 168–179.

Moreira, A. F., Rodrigues, C. F., Reis, C. A., Costa, E. C., Ferreira, P., & Correia, I. J. (2018). Development of poly-2-ethyl-2-oxazoline coated gold-core silica shell nanorods for cancer chemo-photothermal therapy. *Nanomedicine*, *13*(20), 2611–2627.

Nikoobakht, B., & El-Sayed, M. A. (2003). Preparation and growth mechanism of gold nanorods (NRs) using seed-mediated growth method. *Chemistry of Materials*, *15*(10), 1957–1962.

Pelaz, B., del Pino, P., Maffre, P., Hartmann, R., Gallego, M., Rivera-Fernández, S., de la Fuente, J. M., Nienhaus, G. U., & Parak, W. J. (2015). Surface functionalization of nanoparticles with polyethylene glycol: Effects on protein adsorption and cellular uptake. *ACS Nano*, *9*(7), 6996–7008.

Reis, C. A., Rodrigues, C. F., Moreira, A. F., Jacinto, T. A., Ferreira, P., & Correia, I. J. (2019). Development of gold-core silica shell nanospheres coated with poly-2-ethyl-oxazoline and β-cyclodextrin aimed for cancer therapy. *Materials Science and Engineering: C*, *98*, 960–968.

Rodrigues, C. F., Jacinto, T. A., Moreira, A. F., Costa, E. C., Miguel, S. P., & Correia, I. J. (2019). Functionalization of AuMSS nanorods towards more effective cancer therapies. *Nano Research*, *12*(4), 719–732.

Rodrigues, C. F., Reis, C. A., Moreira, A. F., Ferreira, P., & Correia, I. J. (2019). Optimization of gold core-mesoporous silica shell functionalization with TPGS and PEI for cancer therapy. *Microporous and Mesoporous Materials*, *285*, 1–12.

Shen, S., Tang, H., Zhang, X., Ren, J., Pang, Z., Wang, D., Gao, H., Qian, Y., Jiang, X., & Yang, W. (2013). Targeting mesoporous silica-encapsulated gold nanorods for chemo-photothermal therapy with near-infrared radiation. *Biomaterials*, *34*(12), 3150–3158.

Su, C., Li, J., Zhang, L., Wang, H., Wang, F., Tao, Y., Wang, Y., Guo, Q., Li, J., Liu, Y., Yan, Y., & Zhang, J. (2020). The biological functions and clinical applications of integrins in cancers. *Frontiers in Pharmacology*, *11*, 1435.

Wang, K., Zhang, Y., Wang, J., Yuan, A., Sun, M., Wu, J., & Hu, Y. (2016). Self-assembled IR780-loaded transferrin nanoparticles as an imaging, targeting and PDT/PTT agent for cancer therapy. *Scientific Reports*, *6*(1), 1–11.

Yang, J., Luo, Y., Xu, Y., Li, J., Zhang, Z., Wang, H., Shen, M., Shi, X., & Zhang, G. (2015). Conjugation of iron oxide nanoparticles with RGD-modified dendrimers for targeted tumor MR imaging. *ACS Applied Materials & Interfaces*, *7*(9), 5420–5428.

Yang, X., Yang, M., Pang, B., Vara, M., & Xia, Y. (2015). Gold nanomaterials at work in biomedicine. *Chemical Reviews*, *115*(19), 10410–10488.

Zhou, H., Xu, H., Li, X., Lv, Y., Ma, T., Guo, S., Huang, Z., Wang, X., & Xu, P. (2017). Dual targeting hyaluronic acid-RGD mesoporous silica coated gold nanorods for chemo-photothermal cancer therapy. *Materials Science and Engineering: C*, *81*, 261–270.

SUPPORTING INFORMATION

Additional supporting information may be found in the online version of the article at the publisher's website.

How to cite this article: Gonçalves, A. S. C., Rodrigues, C. F., Fernandes, N., de Melo-Diogo, D., Ferreira, P., Moreira, A. F., & Correia, I. J. (2022). IR780 loaded gelatin-PEG coated gold core silica shell nanorods for cancer-targeted photothermal/photodynamic therapy. *Biotechnology and Bioengineering*, 119, 644–656. https://doi.org/10.1002/bit.27996